Catal Lett (2013) 143:807–816
DOI 10.1007/s10562-013-1024-4

Using Fenton-Reaction as a Novel Approach to Enhance the Photocatalytic Activity of TiO_2-γ-Fe_2O_3 Magnetic Photocatalyst Undergoing Photo-Dissolution Process without Silica Interlayer

Harsha Narayani · Hajara Arayapurath · Satyajit Shukla

Received: 22 February 2013 / Accepted: 10 May 2013 / Published online: 24 May 2013

Abstract The photocatalytic activity of TiO_2-γ-Fe_2O_3 core–shell magnetic photocatalyst is known to be severely affected by the photo-dissolution phenomenon in the absence of SiO_2 interlayer. We demonstrate here that the involvement of advance oxidation process, such as the Fenton-reaction, makes the same photo-dissolution process responsible for an enhanced photocatalytic activity.

Keywords Nanocrystalline · Hydrogen peroxide · Advanced oxidation process · Sol–gel · Stober-process

1 Introduction

Nanocrystalline anatase-titania (TiO_2) is a well-known semiconductor-oxide photocatalyst used for the decomposition of organic synthetic-dyes under the ultraviolet (UV), visible, or solar radiation exposure [1, 2]. Due to the difficulties in the separation of TiO_2-based photocatalysts from the treated aqueous solution, due to their non-magnetic nature, the magnetic photocatalysts have been recently developed [3–5]. The magnetic photocatalyst is a nano-composite which has the "core–shell" structure with the core of a magnetic oxide and the shell of a photocatalyst such as the nanocrystalline anatase-TiO_2 and can be separated from the treated aqueous solution using an external magnetic field (that is, magnetically separable photocatalyst).

The use of magnetite (Fe_3O_4) and maghemite (γ-Fe_2O_3) as a magnetic oxide core in a magnetic photocatalyst has been reported in the literature [6–17]. However, the TiO_2-coated γ-Fe_2O_3 has been demonstrated to exhibit very low photocatalytic activity under the UV-radiation exposure due to two reasons. First, during the processing of TiO_2-coated γ-Fe_2O_3, the calcination treatment conducted at higher temperature causes the Fe^{3+} ions to diffuse into the TiO_2 lattice which then act as trapping and/or annihilating centers for the photo-induced electrons and holes (e^-/h^+), thus enhancing or reducing the photocatalytic activity depending on the concentration of diffused Fe^{3+} ions [18]. Secondly, the Fe^{2+} ions formed via the reduction of Fe^{3+} ions present in the surface of TiO_2 photocatalyst get dissolved into the solution (the photo-dissolution process) during the measurement of photocatalytic activity. These dissolved Fe^{2+} ions can then react with the generated hydroxyl-radicals ($OH^\bullet$) and transform them to hydroxyl-ions (OH^-), thus reducing the photocatalytic activity [19, 20].

In order to avoid the diffusion of Fe^{3+} ions into the TiO_2 lattice during the calcination treatment and to avoid the electronic interaction of the magnetic oxide core and the photocatalyst shell during the photocatalytic activity measurements, the silica (SiO_2) has been normally utilized as an interlayer between the core and the shell which enhances the photocatalytic activity under the UV-radiation exposure [6, 8, 9, 12, 14–17]. In our knowledge, there are no reports in the literature which demonstrate the enhancement in the photocatalytic activity of TiO_2-coated γ-Fe_2O_3 without the interlayer of SiO_2 typically under the occurrence of photo-dissolution process. As a result, increasing the photocatalytic activity of TiO_2-coated γ-Fe_2O_3, in the presence of both the Fe^{3+} ions diffused into the TiO_2 lattice and the

H. Narayani · H. Arayapurath · S. Shukla (✉)
Functional Materials Section (FMS), Materials Science and Technology Division (MSTD), National Institute for Interdisciplinary Science and Technology (NIIST), Council of Scientific and Industrial Research (CSIR), Industrial Estate P.O., Pappanamcode, Thiruvananthapuram, Kerala 695019, India
e-mail: satyajit_shukla@niist.res.in

photo-dissolution of Fe^{2+} ions into the solution under the UV-radiation exposure, without the use of SiO_2 interlayer is a real challenge. Hence, the major objective of this work is set to demonstrate a new approach, by simultaneously involving the advanced oxidation process, to substantially enhance the photocatalytic activity of TiO_2-coated γ-Fe_2O_3 magnetic photocatalyst under the UV-radiation exposure without the use of SiO_2 interlayer.

2 Experimental Section

2.1 Chemicals

Titanium(IV)-isopropoxide ($Ti(OC_3H_7)_4$, 97 %), nano-crystalline γ-Fe_2O_3 (<50 nm, 98 %) tetraethylorthosilicate (TEOS, 98 %), hydrogen peroxide (H_2O_2, 3 wt%), and terephthalic acid (TA, 98 %) were purchased from Sigma-Aldrich Chemicals, Bangalore, India; ammonium hydroxide (NH_4OH, 25 wt%) from Qualigens Fine Chemicals, India; and ethanol (99.9 % AR), 2-propanol (99.5 %, ACS reagent), sodium hydroxide (NaOH, Assay 97 %), methylene blue (MB, 96 %) from S.D. Fine-Chem Ltd., Mumbai, India. All chemicals were used as-received without any further purification and/or modification.

2.2 Sample Preparation

2 g of as-received γ-Fe_2O_3 magnetic particles were suspended in a solution of 0.5 g of $Ti(OC_3H_7)_4$ dissolved in 125 ml of 2-propanol. A solution consisting 0.15 ml of distilled-water ($R = 5$, defined as the ratio of molar concentration of water to that of alkoxide-precursor) dissolved in 125 ml of 2-propanol, was added drop-wise to the above suspension. The resulting suspension was stirred for 12 h using an overhead stirrer (IKA RW 14, Sigma-Aldrich Labware, Bangalore, India) and then separated using a moderate external magnetic field (magnetic separator, Sigma-Aldrich Labware, Bangalore, India) or a centrifuge (R23, Remi Instruments Ltd., Mumbai, India) operated at 3,000 rpm. The separated photocatalyst powder was washed using 100 ml of 2-propanol and then dried in an oven at 60 °C overnight. The sol–gel process was repeated for the different number of cycles (1 and 5) to control the thickness of amorphous-TiO_2 coating which is then converted to anatase-TiO_2 via the calcination treatment (heating rate of 3 °C min^{-1}) of dried-powder at 600 °C for 2 h. (Note: The calcination at 600 °C is required for obtaining 100 % anatase-phase (that is, without any anatase-to-rutile phase transformation) with the crystallinity as high as possible.)

The same procedure was followed to deposit the anatase-TiO_2 on the surface of SiO_2-coated γ-Fe_2O_3. The latter was obtained via modified Stober process [21, 22]. To 2 g suspension of magnetic γ-Fe_2O_3 powder dispersed in 250 ml ethanol, 14.5 ml TEOS was slowly added and stirred for 1 h using an overhead stirrer. This was followed by the drop-wise addition of mixture of 2.5 ml NH_4OH and 63.5 ml distilled-water and the suspension was stirred for 12 h. The resulting product was collected via magnetic separation, washed with 100 ml ethanol and four times using the distilled-water followed by drying in an oven at 60 °C overnight. The calculated amounts of relative weight-fractions of anatase-TiO_2, SiO_2, and Fe_2O_3 in the magnetic photocatalyst particles, processed under the different conditions, are tabulated in Table 1.

2.3 Characterization and Measurements

The morphology of different products were examined using the transmission electron microscope (TEM, Tecnai G^2, FEI, The Netherlands) operated at 300 kV. The nanoparticle size distribution was determined using the Dynamic Light Scattering (DLS, Zetasizer 3000 HAS, Malvern Instruments, UK). The stable suspensions of samples were prepared via dispersing the powders in the aqueous media contained in a 10 mm × 10 mm × 45 mm plastic four clear-wall cuvette. The crystallinity of different samples was confirmed via the selected-area electron diffraction (SAED) technique. The crystalline phases present were determined via the X-ray diffraction (XRD, PW1710 Phillips, The Netherlands) using the Cu $K\alpha$ ($\lambda_{Cu} = 1.542$ Å) X-radiation.

The photocatalytic activity was studied by monitoring the degradation of MB dye in an aqueous suspension under the continuous UV-radiation exposure. 125 ml aqueous (or 3 wt% H_2O_2) suspension was prepared by completely dissolving 7.5 μM of MB dye and then dispersing 0.4 g l^{-1} of magnetic photocatalyst particles. After stirring in dark for 1 h, the stable aqueous suspension was irradiated with the UV-light using a Photoreactor (Luzchem Inc., Canada) containing 16 UVA tubes as the UV-source having the illuminance of 255 lm m^{-2} (lux) and emitting the radiation

Table 1 The weight-fractions (%) of anatase-TiO_2, SiO_2, and Fe_2O_3 in the magnetic photocatalyst particles processed under the different conditions

Phase	Cycle-1		Cycle-5	
	Without SiO_2	With SiO_2	Without SiO_2	With SiO_2
Anatase-TiO_2	6	4	25	17
SiO_2	–	36	–	31
Fe_2O_3	94	60	75	52

The calculations are based on the relative amounts of precursors used during the processing

having the peak-wavelength at ~350 nm. 8 ml aliquot was separated after a definite time interval for obtaining the absorption spectra using the UV–visible absorption spectrophotometer (UV-2401 PC, Shimadzu, Japan) of the filtrate obtained after separating the photocatalyst particles using a magnetic separator or a centrifuge. The normalized concentration of MB dye remaining in the solution was calculated using the equation of the form,

$$\%MB_{adsorbed} = \left(\frac{C_t}{C_0}\right)_{MB} \times 100 \quad (1)$$

which is equivalent of the form,

$$\%MB_{adsorbed} = \left(\frac{A_t}{A_0}\right)_{MB} \times 100 \quad (2)$$

where, C_0 (mg l^{-1}) and C_t (mg l^{-1}) correspond to the MB dye concentration at initial and after the contact time t with the corresponding absorbance of A_0 and A_t.

Free-$OH^{\bullet}$ trapping experiments were performed to trap the free-$OH^{\bullet}$ using the TA which were produced under the continuous UV-radiation exposure of photocatalyst particles in an aqueous (or 3 wt% H_2O_2) suspension. These experiments were similar to the one described above for the photocatalytic activity measurements, except that the MB dye was replaced with 5×10^{-4} M of TA and 2×10^{-3} M NaOH [23, 24]. The trapping of free-$OH^{\bullet}$ by TA results in the formation of 2-hydroxyterephthalic acid which exhibits a characteristic photoluminescence (PL) peak located at ~625 nm at an excitation wavelength of ~315 nm. The intensity of PL peak is regarded as the measure of amount of free-$OH^{\bullet}$ produced at a given time under the UV-radiation exposure.

The photo-dissolution experiments were conducted, under the UV-radiation exposure, of photocatalyst particles in an aqueous suspension. These experiments were similar to the one described above for the photocatalytic activity measurements without the addition of MB dye. After 2 h of UV-radiation exposure, the photocatalyst particles were separated using either a magnetic separator or a centrifuge and the filtrate was then analyzed using the inductively coupled plasma atomic emission spectrometer (ICP-AES, Thermo Electron IRIS INTREPID II XSP DUO) for determining the Fe-content (detection limit of 0.01 ppm). The amount of Fe detected via ICP-AES analysis in pure distilled-water, used for all above experiments, was below the detection limit of the instrument.

3 Results and Discussion

The TEM image of as-received nanocrystalline γ-Fe_2O_3 (maghemite) particles is shown in Fig. 1a. The size of as-received nanocrystalline γ-Fe_2O_3 particles is within the range of 15–30 nm having the near-spherical morphology. The selected-area electron diffraction (SAED) pattern, shown as an inset in Fig. 1a, exhibits a concentric ring pattern indicating the nanocrystalline nature of as-received γ-Fe_2O_3 nanoparticles in agreement with the TEM image. The TEM images of anatase-TiO_2-coated ($\gamma + \alpha$)-Fe_2O_3 and α-Fe_2O_3 (hematite) nanoparticles, obtained after the different sol–gel TiO_2 coating-cycles, are presented in Fig. 1b, c. The nano-composite particles appear to be aggregated and the degree of aggregation is noted to increase with the number of sol–gel TiO_2 coating-cycles. In Fig. 1c, the α-Fe_2O_3 nanoparticles are seen to be embedded in the matrix of nanocrystalline anatase-TiO_2 having the typical core–shell morphology as noted in Fig. 1d. The TiO_2 shell appears to completely cover the α-Fe_2O_3 core. The nanoparticle size distribution for the different samples, as measured using the DLS technique, is shown in Fig. 2. The nanoparticle size distribution appears to be bimodal and unimodal in Fig. 2a–c and Fig. 2d–f. The peak-values of nanoparticle size distribution are tabulated in Table 2. It is noted that the calcination treatment conducted at 600 °C for 2 h enhances the average nanoparticle size of as-received γ-Fe_2O_3. Without the SiO_2 interlayer, a single TiO_2 coating-cycle restricts the particle growth; however, large number of TiO_2 coating-cycles appears to cause the aggregation of nano-composite particles which supports the TEM analysis. In the presence of SiO_2 interlayer, the extent of aggregation is noted to be comparable for lower and higher number of TiO_2 coating-cycles.

The XRD patterns of magnetic oxide particles obtained after the calcination of as-received γ-Fe_2O_3 nanoparticles at 600 °C for 2 h and those of anatase-TiO_2-coated ($\gamma + \alpha$)-Fe_2O_3 (cycle-1) and α-Fe_2O_3 (cycle-5) nano-composite particles, obtained after the calcination treatment with the different sol–gel TiO_2 coating-cycles, are presented in Fig. 3a–c respectively. The calcination treatment has resulted in the complete phase transformation of as-received γ-Fe_2O_3 to α-Fe_2O_3, Fig. 3a. The surface-deposition of increasing amount of anatase-TiO_2, without the SiO_2 interlayer, could not prevent this phase transformation, Fig. 3b–c. The γ-Fe_2O_3 to α-Fe_2O_3 (or $\alpha + \varepsilon$-Fe_2O_3) phase transformation appears to be partial and full for the sol–gel TiO_2 coating-cycles of 1 and 5 which suggests that lower number of sol–gel TiO_2 coating-cycles can effectively prevent the above phase transformation compared with larger number of sol–gel TiO_2 coating-cycles. It is to be noted that the amorphous-TiO_2 is first deposited on the surface of as-received γ-Fe_2O_3 magnetic nanoparticles via the sol–gel process which is then converted to anatase-TiO_2 via the high temperature calcination treatment. The formation of rutile-TiO_2 is not observed in the present investigation which is consistent with our earlier reports [3, 25]. In contrast to this, for the same TiO_2-coated γ-Fe_2O_3 nano-composite system

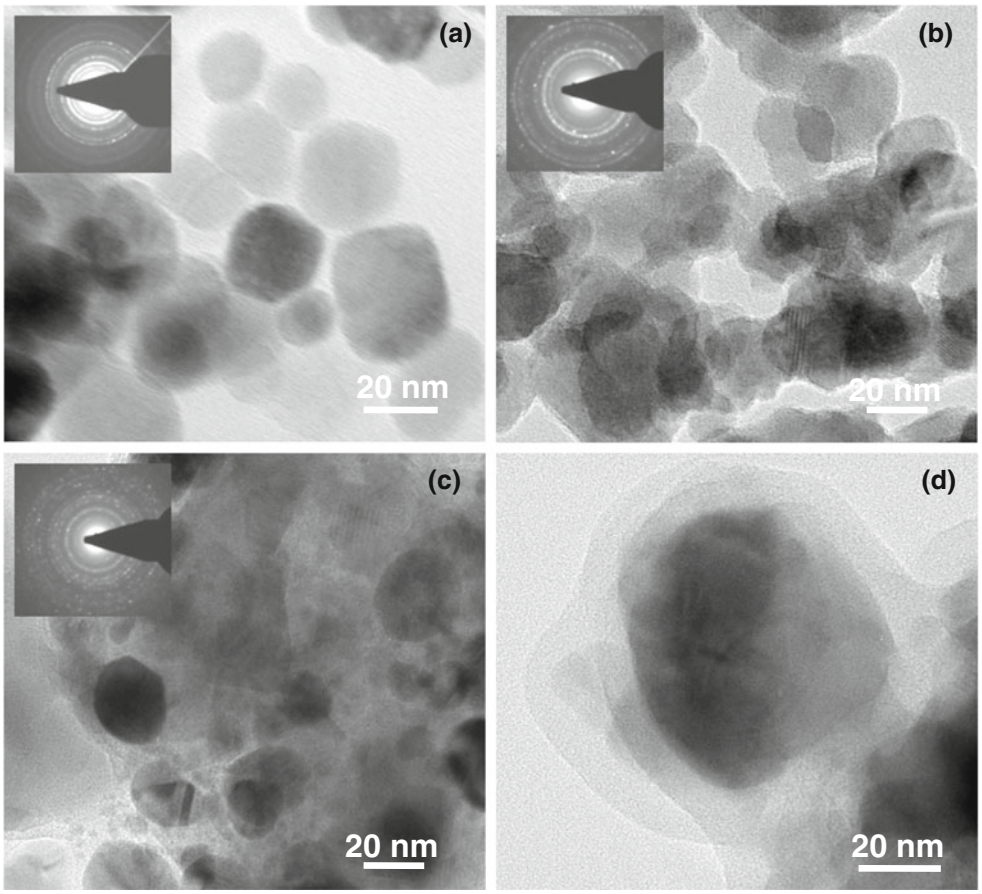

Fig. 1 TEM images of as-received nanocrystalline γ-Fe_2O_3 particles **a**, anatase-TiO_2-coated (γ + α)-Fe_2O_3 **b** and α-Fe_2O_3 **c** nano-composite particles obtained via different number of sol–gel TiO_2-coating cycles 1 **b** and 5 **c**. In **d**, the core–shell morphology of anatase-TiO_2-coated α-Fe_2O_3 nano-composite particle is clearly visible. The dark-gray and light-gray contrasts represent α-Fe_2O_3 as a core and anatase-TiO_2 as a shell

with the almost identical composition, a complete transformation of anatase-TiO_2 to rutile-TiO_2 has been reported [26] where the shell of nanocrystalline TiO_2 has been derived using the precipitation method involving the $TiOSO_4$ precursor. Hence, the stabilization of anatase-TiO_2 after the calcination at 600 °C appears to be governed by the technique and the precursor utilized for the processing of magnetic nano-composite particles. Moreover, the porous nature of amorphous-TiO_2 coating may not avoid the access of γ-Fe_2O_3 to the atmospheric oxygen during the calcination treatment which results in the partial phase transformation of magnetic oxide core [10]. In addition to this, since the γ-Fe_2O_3 to α-Fe_2O_3 phase transformation begins at the surface [27], the stability of interphase boundary between the amorphous-TiO_2 and γ-Fe_2O_3 plays a crucial role in the nucleation and growth of α-Fe_2O_3. Since the sol–gel derived TiO_2 undergoes a phase transformation from amorphous-to-anatase at about 400 °C [25], the interphase boundary between the amorphous-TiO_2 and γ-Fe_2O_3 becomes weaker due to the atomic rearrangement taking place within the amorphous-TiO_2 at the interphase boundary which allows the easy nucleation and growth of α-Fe_2O_3 phase. Hence, both the porous nature of amorphous-TiO_2 and the amorphous-to-anatase phase transformation in TiO_2 at 400 °C are responsible for the observed phase transformation of magnetic oxide core in the presence of TiO_2-coating during the calcination treatment at 600 °C. For the TiO_2 coating obtained via a single sol–gel coating-cycle, greater resistance to the amorphous-to-anatase phase transformation is observed, Fig. 3b, due to the strong interaction of the substrate with the TiO_2 coating as a consequence of smaller thickness of the latter. The dominance of this substrate-effect on the amorphous-to-anatase phase transformation is also possibly responsible for the partial stabilization of γ-Fe_2O_3, Fig. 3b. However, for the TiO_2 coating obtained via the multiple sol–gel coating-cycles, the substrate-effect is reduced drastically which is reflected not only in the complete amorphous-to-anatase phase transformation but also in the complete γ-Fe_2O_3 to α-Fe_2O_3 (or α + ε-Fe_2O_3) phase transformation, Fig. 3c. This strongly suggests the easy diffusion of atmospheric oxygen through the TiO_2 coating having

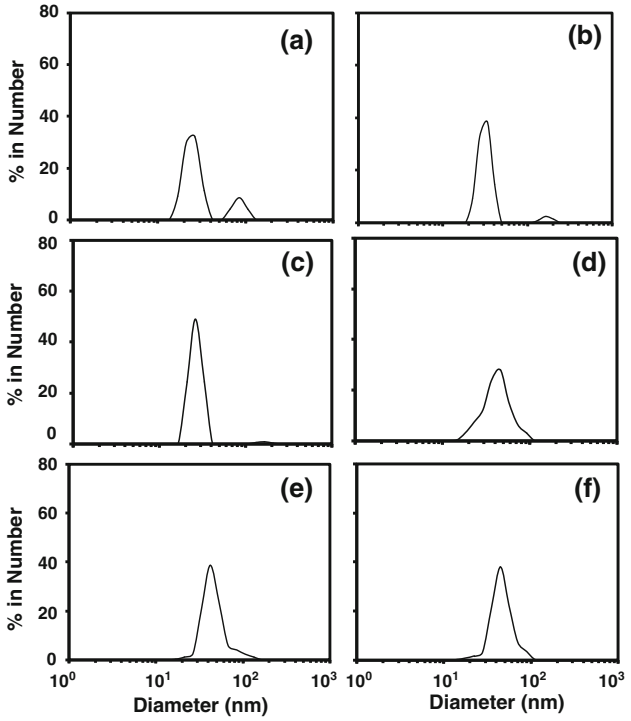

Fig. 2 Nanoparticle size distribution curves as obtained for the different samples using the DLS technique as-received γ-Fe_2O_3 **a**, α-Fe_2O_3 (calcined) **b**, anatase-TiO_2-coated ($\gamma + \alpha$)-Fe_2O_3 **c** and α-Fe_2O_3 **d** nano-composite particles obtained using the sol–gel TiO_2-coating cycles of 1 **c** and 5 **d**, and anatase-TiO_2-coated SiO_2/γ-Fe_2O_3 nano-composite particles obtained using the sol–gel TiO_2-coating cycles of 1 **e** and 5 **f**

Table 2 The peak-values of nanoparticle size distribution (nm) as obtained for the different samples using the DLS technique

Sample	First major peak (second minor peak)
γ-Fe_2O_3 (maghemite)	266 (842)
α-Fe_2O_3 (hematite)	333 (1653)
Anatase-TiO_2-coated (cycle-1) ($\gamma + \alpha$)-Fe_2O_3	263 (1661)
Anatase-TiO_2-coated (cycle-5) α-Fe_2O_3	459 (–)
Anatase-TiO_2-coated (cycle-1) SiO_2/γ-Fe_2O_3	423 (–)
Anatase-TiO_2-coated (cycle-5) SiO_2/γ-Fe_2O_3	443 (–)

higher thickness which can also possibly lead to the formation of an intermediate ε-Fe_2O_3 phase at the interphase boundary [28]. With the introduction of SiO_2 interlayer in between the core and the shell, however, the above phase transformation could be prevented completely, Fig. 4, due to the following two reasons. Firstly, the highly dense SiO_2 interlayer does not allow the atmospheric oxygen to contact the magnetic oxide core; and secondly, the SiO_2 interlayer does not encounter any phase transformation within the temperature range investigated here making the interphase boundary between SiO_2 and γ-Fe_2O_3 more stable which in turn does not allow the easy nucleation of α/ε-Fe_2O_3. As a result, although the amorphous-to-anatase phase transformation occurs in the presence of SiO_2 interlayer, the core of γ-Fe_2O_3 phase remains untransformed.

The average nanocrystallite size of different phases present in the magnetic oxide and nano-composite particles, processed under the different conditions, are tabulated in the Table 3. The calcination of pure γ-Fe_2O_3 at 600 °C for 2 h results not only in the phase transformation to α-Fe_2O_3 but also in the growth of the average nanocrystallite size. This increase in the average nanocrystallite size of magnetic oxide core is restricted in the presence of SiO_2 and TiO_2 coatings. This restriction further appears to be relatively higher when the amount of amorphous-to-anatase phase transformation is limited and SiO_2 interlayer is present.

The variation in the normalized residual MB dye concentration as a function of UV-radiation exposure time in pure H_2O, as obtained for the anatase-TiO_2-coated (cycle-1) ($\gamma + \alpha$)-Fe_2O_3 and γ-Fe_2O_3 nano-composite particles processed without and with the SiO_2 interlayer, is presented in Fig. 5a. Similar variation as obtained for the anatase-TiO_2-coated (cycle-1) ($\gamma + \alpha$)-Fe_2O_3 nano-composite particles in 1 M H_2O_2 is also shown. The corresponding qualitative variation in the concentration of $OH^{\bullet}$ produced as a function of UV-radiation exposure time, as obtained via the PL analysis under the above test-conditions, is presented in Fig. 6. As observed in Fig. 5a, the anatase-TiO_2-coated (cycle-1) ($\gamma + \alpha$)-Fe_2O_3 nano-composite particles do not exhibit any photocatalytic activity ($k_{app} = 0$ min^{-1}) in pure H_2O. This has been attributed to the photo-induced e^-/h^+ pair transfer from the anatase-TiO_2 to ($\gamma + \alpha$)-Fe_2O_3 and their lower mobility in ($\gamma + \alpha$)-Fe_2O_3 resulting in the rapid rate of recombination which is aided by narrower band-gap energy values of these semiconductor oxides [6, 7]. Since the conduction-band and valence-band energy levels of anatase-TiO_2 are higher and lower than those of ($\gamma + \alpha$)-Fe_2O_3 respectively [7], the photo-induced e^-/h^+ pairs generated in the anatase-TiO_2 can easily escape into ($\gamma + \alpha$)-Fe_2O_3 nanoparticles and get annihilated before they can produce the $OH^{\bullet}$ in the surrounding aqueous solution which are responsible for the degradation of MB dye. As a result, for the anatase-TiO_2-coated (cycle-1) ($\gamma + \alpha$)-Fe_2O_3 nano-composite particles, the concentration of $OH^{\bullet}$ produced is significantly lower as observed in Fig. 6a. Moreover, it is to be noted that under an exposure to the UV-radiation, the photo-induced electrons in the anatase-TiO_2 result in the formation of Fe^{2+} ions via the reduction of Fe^{3+} ions which are already diffused into the anatase-TiO_2 lattice during the calcination treatment. For the present sample, due to the smallest thickness of anatase-TiO_2 shell as obtained via a single sol–gel TiO_2 coating-cycle, the former is highly concentrated

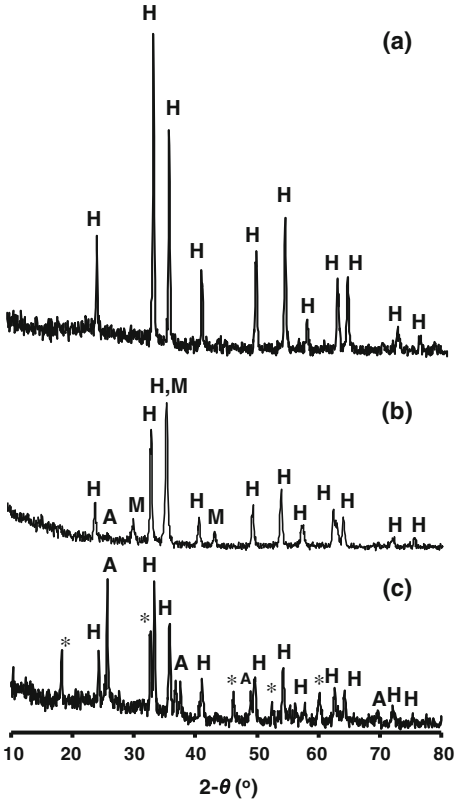

Fig. 3 XRD patterns of nanocrystalline α-Fe_2O_3 particles (obtained after the calcination of nanocrystalline γ-Fe_2O_3 particles at 600 °C for 2 h) **a**, anatase-TiO_2-coated (γ + α)-Fe_2O_3 **b** and α-Fe_2O_3 **c** nano-composite particles obtained via different number of sol–gel TiO_2-coating cycles 1 **b** and 5 **c**. M, H, and A represent the maghemite (γ-Fe_2O_3), hematite (α-Fe_2O_3), and anatase structures respectively. In **b**, the weight-fraction of α-Fe_2O_3 is calculated to be 64 %. In **c**, the peaks marked with *asterisk* are attributed to the possible presence of an intermediate ε-Fe_2O_3 phase [28]

with the diffused Fe^{3+} cations after the calcination treatment at 600 °C for 2 h. Due to their larger size the Fe^{2+} ions, which are newly formed at the surface under the UV-radiation exposure, get immediately dissolved into the surrounding aqueous solution [7, 11] (termed here as the "photo-dissolution process"). The Fe^{2+} ions thus generated in an aqueous solution, however, can decrease the concentration of $OH^{\bullet}$ produced via the following reaction [19, 20].

$$Fe^{2+} + OH^{\cdot} \rightarrow Fe^{3+} + OH^{-} \quad (3)$$

The amount of photo-dissolved Fe for the present sample is 0.89 ppm which is ~30 times larger than that (0.03 ppm) observed for the as-received γ-Fe_2O_3 nanoparticles. Hence, the photo-dissolved Fe^{2+} ions do play a major role in minimizing both the concentration of $OH^{\bullet}$ produced by this sample, and hence, its photocatalytic activity, Fig. 5a.

In order to enhance the photocatalytic activity of anatase-TiO_2-coated (cycle-1) (γ + α)-Fe_2O_3 nano-composite

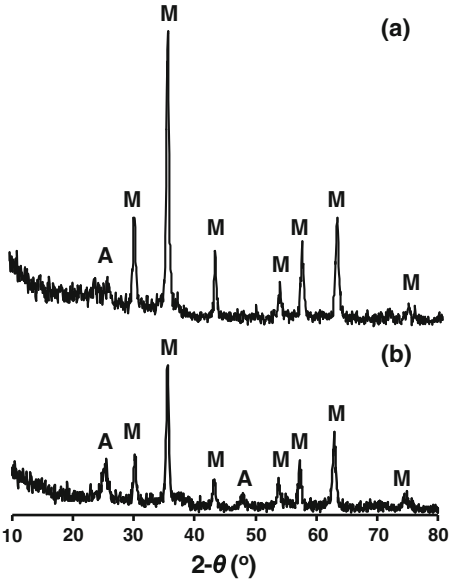

Fig. 4 XRD patterns of anatase-TiO_2-coated SiO_2/γ-Fe_2O_3 nano-composite particles obtained via different number of sol–gel TiO_2-coating cycles 1 **a** and 5 **b**. M and A represent the maghemite (γ-Fe_2O_3) and anatase structures

particles, two different approaches are investigated here. In the first approach, the amorphous-SiO_2 is introduced as an interlayer between the magnetic oxide core and the anatase-TiO_2 shell. Since the band-gap energy of amorphous-SiO_2 is larger (9.0 eV) with its conduction-band and valence-band energy levels above and below those of anatase-TiO_2 [29–31], it significantly hinders the transfer of photo-induced e^-/h^+ pairs from the anatase-TiO_2 to γ-Fe_2O_3. As a result, a drastic increase in the concentration of $OH^{\bullet}$ produced is noted after the introduction of SiO_2 interlayer, Fig. 6b, due to the following redox reactions taking place on the surface of nano-composite particles with the corresponding increase in the dye-degradation kinetics ($k_{app} = 0.02\ min^{-1}$), Fig. 5a [25].

$$TiO_2 + h\nu \rightarrow e^- + h^+ \quad (4)$$

$$OH^- + h^+ \rightarrow OH^{\cdot} \quad (5)$$

$$O_2 + e^- \rightarrow O_2^- \quad (6)$$

$$2O_2^- + 2H^+ \rightarrow H_2O_2 + O_2 \quad (7)$$

$$H_2O_2 + e^- \rightarrow OH^{\cdot} + OH^- \quad (8)$$

The amount of photo-dissolved Fe, in the case of anatase-TiO_2-coated (cycle-1) SiO_2/γ-Fe_2O_3 nanoparticles, is measured to be 0.03 ppm which is equal to that obtained for the as-received γ-Fe_2O_3 nanoparticles. Hence, for the present sample, the effect of photo-dissolution of Fe^{2+} on the photocatalytic activity can be assumed to be minimum. The enhancement in the photocatalytic activity is, hence, attributed to the effect of interlayer SiO_2 in agreement with

Table 3 Average nanocrystallite size (nm) of different phases present in the magnetic photocatalyst particles processed under the different conditions as derived using the well-known Scherrer equation

Phase	Pure	Cycle-1		Cycle-5	
		Without SiO_2	With SiO_2	Without SiO_2	With SiO_2
γ-Fe_2O_3 (maghemite)	20	22	18	–	16
α-Fe_2O_3 (hematite)	35	23	–	30	–
Anatase-TiO_2	–	22	41	28	9

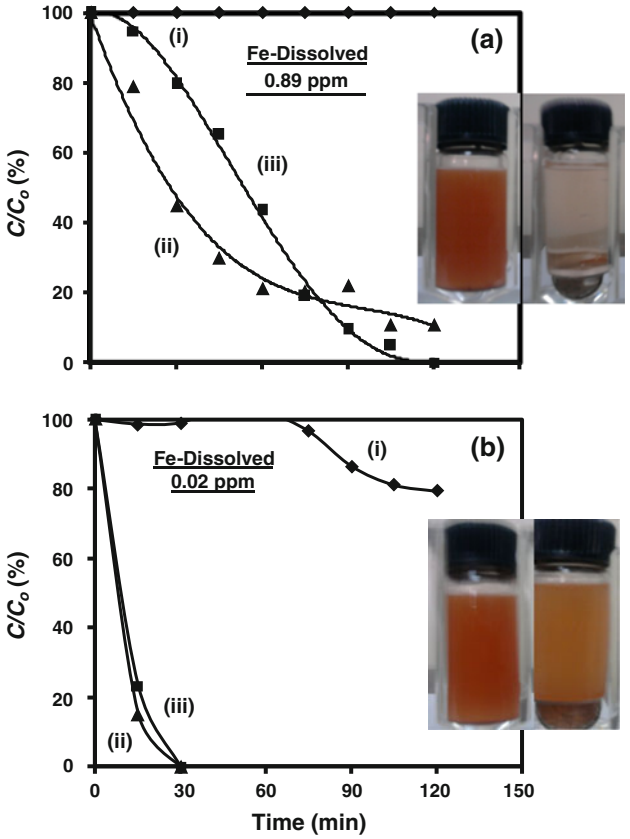

Fig. 5 Variation in the normalized residual MB dye concentration as a function of UV-radiation exposure time as obtained for the anatase-TiO_2-coated ($\gamma + \alpha$)-Fe_2O_3, γ-Fe_2O_3, and α-Fe_2O_3 nano-composite particles processed with different number of sol–gel TiO_2 coating-cycles 1 **a** and 5 **b**. *i* and *iii* correspond to the samples processed without the SiO_2 interlayer; while, *ii* corresponds to those processed with the SiO_2 interlayer. The photocatalytic activity measurements are conducted in pure H_2O *i*, *ii* and $\sim$1 M H_2O_2 *iii*

the several other reports in the literature which show an increase in the photocatalytic activity obtained via the introduction of SiO_2 as an interlayer between the magnetic oxide core and the photocatalyst shell. The SiO_2 interlayer avoids not only the diffusion of Fe^{3+} ions from the core to the shell during the calcination treatment but also the electronic interaction between the two during the measurement of photocatalytic activity under the UV-radiation exposure [6, 8, 9, 12, 14–17]. In support of this, the concentration of $OH^{\bullet}$ produced by the anatase-TiO_2-coated (cycle-1) SiO_2/γ-Fe_2O_3 nanoparticles is noted to be higher and also to increase gradually with the UV-radiation exposure time, Fig. 6b.

In the second approach which is novel to enhance the photocatalytic activity of anatase-TiO_2-coated (cycle-1) ($\gamma + \alpha$)-Fe_2O_3 nano-composite particles, the photocatalytic activity measurements are conducted in $\sim$1 M H_2O_2 solution without the SiO_2 interlayer. It is well-known that the concentration of $OH^{\bullet}$ produced in an aqueous solution can be enhanced via the following "Fenton-reaction" even without an exposure to the external UV-radiation [19, 20].

$$Fe^{2+} + H_2O_2 \rightarrow Fe^{3+} + OH^- + OH^{\cdot} \quad (9)$$

It appears that the addition of H_2O_2 to an aqueous solution is beneficial in increasing the concentration of $OH^{\bullet}$ produced during the simultaneous occurrence of photo-dissolution of Fe^{2+} ions under the UV-radiation exposure. As mentioned earlier, the amount of photo-dissolved Fe, in the case of anatase-TiO_2-coated (cycle-1) ($\gamma + \alpha$)-Fe_2O_3 nano-composite particles, is very high (0.89 ppm). Interestingly, the same sample exhibits very high MB dye degradation kinetics ($k_{app} = 0.023$ min^{-1}) in $\sim$1 M H_2O_2 solution which is comparable with that ($k_{app} = 0.02$ min^{-1}) obtained in pure H_2O via the introduction of SiO_2 interlayer and significantly larger than that ($k_{app} = 0$ min^{-1}) obtained in pure H_2O without the use of SiO_2 interlayer, Fig. 5a. In support of this, the concentration of $OH^{\bullet}$ produced is seen to increase gradually in the first 60 min of UV-radiation exposure time, Fig. 6c, for the anatase-TiO_2-coated (cycle-1) ($\gamma + \alpha$)-Fe_2O_3 nano-composite particles in $\sim$1 M H_2O_2. However, it tends to decrease thereafter with further increase in the UV-radiation exposure time within the interval of 60–120 min (not shown in Fig. 6c for clarity) due to the consumption of $OH^{\bullet}$ produced as a result of their interaction with the Fe^{3+} cations and H_2O_2, Eqs. 3 and 10 [19, 20].

$$OH^{\cdot} + H_2O_2 \rightarrow OOH^{\cdot} + H_2O \quad (10)$$

The nanocrystalline γ-Fe_2O_3 particles are ferrimagnetic with the saturation magnetization of 74 emu g^{-1} and α-Fe_2O_3 nanoparticles are ferromagnetic with the saturation magnetization of 0.57 emu g^{-1} [10]. As a result, the anatase-TiO_2-coated (cycle-1) ($\gamma + \alpha$)-Fe_2O_3 nano-composite particles, consisting of mixed γ-Fe_2O_3 and α-Fe_2O_3 as magnetic oxide

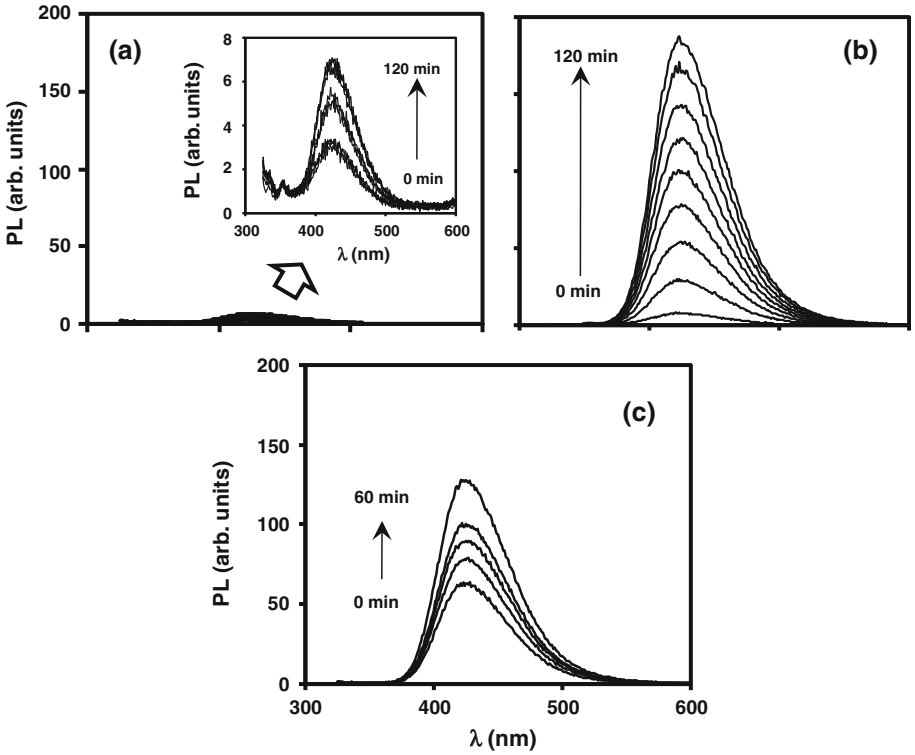

Fig. 6 Variation in the PL intensity associated with the formation of 2-hydroxyterephthalic acid as a function of UV-radiation exposure time as obtained for the anatase-TiO_2-coated (cycle-1) ($\gamma + \alpha$)-Fe_2O_3 **a**, **c** and γ-Fe_2O_3 **b** nano-composite particles. **a** and **c** correspond to the samples processed without the SiO_2 interlayer; while, **b** corresponds to the sample processed with the SiO_2 interlayer. The PL measurements are conducted in pure H_2O **a**, **b** and $\sim$1 M H_2O_2 **c**

core, could be quickly separated from an aqueous solution using a moderate external magnetic field as shown in the right-side inset of Fig. 5a.

Similar to the previous case, the photocatalytic activity measurements are also conducted using the anatase-TiO_2-coated (cycle-5) α-Fe_2O_3 or γ-Fe_2O_3 nano-composite particles, without and with the SiO_2 interlayer, in pure H_2O and $\sim$1 M H_2O_2 solution. The corresponding photocatalytic activity graphs are presented in Fig. 5b. It is again noted that the dye-degradation kinetics ($k_{app} = 0.1$ min^{-1}) obtained using the anatase-TiO_2-coated (cycle-5) α-Fe_2O_3 nano-composite particles in $\sim$1 M H_2O_2 solution is comparable with that ($k_{app} = 0.13$ min^{-1}) obtained in pure H_2O using the SiO_2 interlayer. Moreover, the use of $\sim$1 M H_2O_2 solution is also seen to enhance significantly the photocatalytic activity of anatase-TiO_2-coated (cycle-5) α-Fe_2O_3 nano-composite particles relative to that ($k_{app} = 0.001$ min^{-1}) obtained in pure H_2O. In this case well, although the Fenton-reaction, Eq. 9, is held responsible for an enhanced photocatalytic activity, it differs from the previous case in the manner it takes place under the UV-radiation exposure. For the present sample, the thickness of anatase-TiO_2 shell is relatively larger than that in the previous case due to the more number of sol–gel TiO_2 coating-cycles involved, Fig. 1. Due to the increased diffusion distance, the amount of Fe-dissolved into the solution under the UV-radiation exposure is hence measured to be as low as 0.02 ppm. This suggests that for the present sample, the anatase-TiO_2 shell remains highly doped with Fe^{3+} ions during the photocatalytic activity measurements. It is known that if the concentration of Fe^{3+} ions doped in the nanocrystalline anatase-TiO_2 is either below or above a critical value, then they act either as trapping or annihilating sites for the photo-induced e^-/h^+ pairs [18]. Lower photocatalytic activity of anatase-TiO_2-coated (cycle-5) α-Fe_2O_3 nano-composite particles as observed in pure H_2O, Fig. 5b, is hence contributed by the doped-Fe^{3+} ions which possibly act as annihilating centers for the photo-induced e^-/h^+ pairs. However, in the presence of $\sim$1 M H_2O_2 in the surrounding medium, it appears that the same doped-Fe^{3+} cations, typically present at the surface, act as effective trapping sites and transfer the photo-induced electrons to H_2O_2 within the solution to produce large concentration of $OH^\bullet$, Eq. 9. The generated $OH^\bullet$ are then responsible for an enhanced photocatalytic activity of anatase-TiO_2-coated (cycle-5) α-Fe_2O_3 nano-composite particles. The dynamics in the variation of the concentration of $OH^\bullet$ produced, as observed earlier in Fig. 6a, is also noted for the present sample in pure H_2O and 1 M H_2O_2 solution, Fig. 7a, c. Since the Fe^{3+} diffusion into the anatase-TiO_2 is possible only without the SiO_2 interlayer, it appears that the oscillating variation in the concentration of $OH^\bullet$ produced, as observed for the two different samples processed without the SiO_2 interlayer, further supports the generation of $OH^\bullet$ via the Fenton-reaction either in the presence of photo-dissolution process or in the presence of Fe^{3+}/Fe^{2+} cations on the surface of nano-composite particles. As shown in the

inset of Fig. 5b, the present sample could not be separated using an external magnetic field due to the presence of only α-Fe_2O_3 which has the minimum saturation magnetization.

It is noted that the weight-fraction of anatase-TiO_2 is not same for a specific number of sol–gel TiO_2 coating-cycles (either 1 or 5) when a given amount of magnetic nano-composite particles are processed without and with the SiO_2 interlayer, Table 1. The amount of anatase-TiO_2 in the shell is always higher when the magnetic photocatalyst is processed without the interlayer of SiO_2 compared with that processed with the interlayer of SiO_2. Nevertheless, in spite of higher amount of anatase-TiO_2 the photocatalytic activity of magnetic nano-composite, processed without the SiO_2 interlayer, is almost negligible in the absence of Fenton-reaction for both the number of sol–gel TiO_2 coating-cycles, Fig. 5a, b. Hence, the difference in the weight-fraction of anatase-TiO_2 does not appear to be a critical factor in determining the observed difference in the photocatalytic activity under the given test-conditions. Since the main purpose here is to demonstrate the combined effect of photo-dissolution and Fenton-reaction, the effect of difference in the amount of anatase-TiO_2 within the shell of magnetic nano-composite particles, processed without and with the SiO_2 interlayer, has been neglected.

In addition to this, the concentration of H_2O_2 within the solution is also an important parameter which needs to be considered in further detail to understand precisely the combined effect of photo-dissolution and Fenton-reaction on the photocatalytic activity. It is anticipated that with the same amount of TiO_2 the photocatalytic activity would be relatively superior when the measurements are conducted in pure H_2O with the use of SiO_2 interlayer than those conducted in 3 wt% H_2O_2 without the use of SiO_2 interlayer. However, the results may significantly differ if the concentration of H_2O_2 is increased above 3 wt%. In the authors' view, the precise measurements with the same amount of TiO_2 are, hence, beyond the scope of this investigation due to the other variables involved.

Overall, it is clearly shown here that the addition of H_2O_2 during the photocatalytic activity measurements of anatase-TiO_2-coated ($\gamma + \alpha$)-Fe_2O_3 or α-Fe_2O_3 magnetic nano-composite particles, under the UV-radiation exposure, is beneficial to utilize the photo-dissolution process as a source of Fe^{2+} ions within the solution leading to the large concentration of $OH^{\bullet}$ produced, and hence higher photocatalytic activity, via the Fenton-reaction which is an advanced oxidation process [32, 33]. Thus, the present work when combined with the reports available in the literature would allow to increase the photocatalytic activity of anatase-TiO_2-coated ($\gamma + \alpha$)-Fe_2O_3 or α-Fe_2O_3 magnetic nano-composite particles, under the UV-radiation exposure, without and with the occurrence of photo-dissolution phenomenon. In other words, the addition of H_2O_2 in the surrounding medium is a new alternative for the conventional use of SiO_2 interlayer.

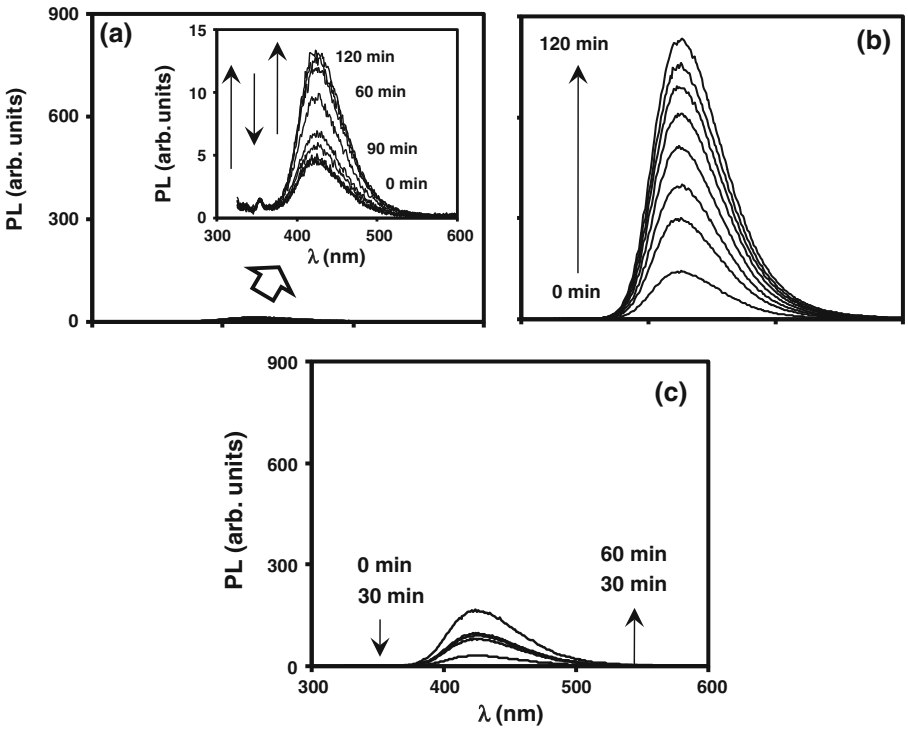

Fig. 7 Variation in the PL intensity associated with the formation of 2-hydroxyterephthalic acid as a function of UV-radiation exposure time as obtained for the anatase-TiO_2-coated (cycle-5) α-Fe_2O_3 **a**, **c** and γ-Fe_2O_3 **b** nano-composite particles. **a** and **c** correspond to the samples processed without the SiO_2 interlayer; while, **b** corresponds to the sample processed with the SiO_2 interlayer. The PL measurements are conducted in pure H_2O **a**, **b** and $\sim$1 M H_2O_2 **c**

4 Conclusions

The anatase-TiO_2-coated (cycle-1 and 5) ($\gamma + \alpha$)-Fe_2O_3 and α-Fe_2O_3 nano-composites particles (magnetic and non-magnetic) exhibit very low photocatalytic activity under the UV-radiation exposure which has been contributed by either the photo-dissolution of Fe^{2+} ions into the solution or the doping of TiO_2 with Fe^{3+} ions in large concentration. Both of the latter effects reduce substantially the concentration of $OH^{\bullet}$ produced under the UV-radiation exposure, and hence, the photocatalytic activity. However, the addition of H_2O_2 to the surrounding aqueous medium significantly enhances the concentration of $OH^{\bullet}$ produced under the UV-radiation exposure, and hence the photocatalytic activity, via the advanced oxidation process involving the Fenton-reaction. Within the investigated range of experimental parameters, the photocatalytic activity is observed to be comparable with that obtained using the SiO_2 interlayer. Thus, the photo-dissolution process which severely affects the photocatalytic activity in the absence of SiO_2 interlayer, is beneficial in enhancing the same when combined with the Fenton-reaction.

Acknowledgments Authors thank CSIR, India for the financial support (Projects # OLP216339 and P81113). Authors also thank Mr. Kiran (Icon Analytical, India), Mr. P. Guruswamy, Mr. Peermohamed (both NIIST-CSIR, India), and Sophisticated Test and Instrumentation Center (STIC), Cochin University of Science and Technology (CUSAT, India) for conducting the TEM/SAED, XRD, PL, and ICP-AES analyses respectively.

References

1. Kumar SG, Devi LG (2011) J Phys Chem A 115:13211
2. Fujishima A, Rao TN, Tryk DA (2000) J Photochem Photobiol C 1:1
3. Thazhe L, Shereef A, Shukla S, Reshmi CP, Varma MR, Suresh KG, Patil K, Warrier KGK (2010) J Am Ceram Soc 93:3642
4. Xu S, Shangguan W, Yuan L, Shi J, Chen M (2007) Sci Technol Adv Mater 8:40
5. Fu W, Yang H, Li M, Chang L, Yu Q, Xu J, Zou G (2006) Mater Lett 60:2723
6. Chen F, Zhao J (1999) Catal Lett 58:245
7. Beydoun D, Amal R, Low GKC, McEvoy S (2000) J Phys Chem B 104:4387
8. Chen F, Xie Y, Zhao J, Lu G (2001) Chemosphere 44:1159
9. Beydoun D, Amal R, Scott J, Low GKC, McEvoy S (2001) Chem Eng Technol 24:7
10. Beydoun D, Amal R (2002) Mater Sci Eng B 94:71
11. Beydoun D, Amal R, Low GKC, McEvoy S (2002) J Mol Catal 180:193
12. Watson S, Beydoun D, Amal R (2002) J Photochem Photobiol A 148:303
13. Gao Y, Chen B, Li H, Ma Y (2003) Mater Chem Phys 88:348
14. Xu MW, Bao SJ, Zhang XG (2005) Mater Lett 59:2194
15. Watson S, Scott J, Beydoun D, Amal R (2005) J Nanopart Res 7:691
16. Song X, Gao L (2005) J Am Ceram Soc 90:4015
17. Gad-Allah TA, Kato S, Satokawa S, Kojima T (2007) Solid State Sci 9:737
18. Zhang Z, Wang CC, Zakaria R, Ying JY (1998) J Phys Chem B 102:10871
19. Gonzalez KC, Lopez OT, Leon AG, Mar JLG, Reyes LH, Ramirez AH, Hernand JMP (2010) Chem Eng J 160:199
20. Jeong J, Yoon J (2005) Water Res 39:2893
21. Lee SW, Drwiega J, Mazyck D, Wu CY, Sigmund WM (2006) Mater Chem Phys 96:483
22. Deng YH, Wang CC, Hu JH, Yang WL, Fu SK (2005) Colloids Surf A 262:87
23. Ishibashi KI, Fujishima A, Watanabe T, Hashimoto K (2000) J Photochem Photobiol 134:139
24. Hirakawa T, Nosaka Y (2002) Langmuir 18:3247
25. Baiju KV, Shukla S, Sandhya KS, James J, Warrier KGK (2007) J Phys Chem C 111:7612
26. Tyrpekl V, Vejpravova JP, Roca AG, Murafa N, Szatmary L, Niznansky D (2011) Appl Surf Sci 257:4844
27. Lagoeiro LE (1998) J Metamorphic Geol 16:415
28. Vales V, Vejpravova JP, Holy V, Tyrpekl V, Brazda P, Doyle S (2010) Phys Status Solidi C 7:1399
29. Zhang X, Yang H, Zhang F, Chan KY (2007) Mater Lett 61:2231
30. Samos LM, Bussi G, Ruini A, Molinari E, Caldas MJ (2011) Phys Status Solidi B 248:5
31. Cho K, Chang H, Park JH, Kim BG, Jang HD (2008) J Ind Eng Chem 14:860
32. Munter R (2001) Proc Est Acad Sci Chem 50:59
33. Zazo JA, Casas JA, Mohedano AF, Gilarranz MA, Rodriguez JJ (2005) Environ Sci Technol 39:9295